AIP Journal of Applied Physics

# Nanocrystal growth and morphology of PbTeSe-ZnSe composite thin films prepared by one-step synthesis method

Kazuhisa Sato and Seishi Abe

Citation: Journal of Applied Physics **120**, 155301 (2016); doi: 10.1063/1.4964874
View online: http://dx.doi.org/10.1063/1.4964874
View Table of Contents: http://scitation.aip.org/content/aip/journal/jap/120/15?ver=pdfcov
Published by the AIP Publishing

# Nanocrystal growth and morphology of PbTeSe-ZnSe composite thin films prepared by one-step synthesis method

Kazuhisa Sato[1,a)] and Seishi Abe[2]
[1]*Institute for Materials Research, Tohoku University, Sendai 980-8577, Japan*
[2]*Research Institute for Electromagnetic Materials, Sendai 982-0807, Japan*

(Received 19 August 2016; accepted 4 October 2016; published online 17 October 2016)

The microstructure of polycrystalline $PbTe_{1-x}Se_x$-ZnSe composite thin films has been studied by scanning transmission electron microscopy and electron diffraction. The films were prepared by the one-step synthesis method using simultaneous evaporation of PbTe and ZnSe. The nanocrystals of $PbTe_{1-x}Se_x$ are formed in a ZnSe matrix. Tellurium concentration can be tuned by controlling the PbTe evaporation source temperatures between 753 K and 793 K. Binary PbSe nanocrystals were formed at 753 K, while ternary $PbTe_{1-x}Se_x$ nanocrystals were formed at 793 K. The nanocrystals grow in a granular shape at the initial stage of film growth, and the morphology changes to nanowire-shape as the film grows, irrespective of the Te concentration. The ternary $PbTe_{1-x}Se_x$ nanocrystals were composed of two phases with different Te concentration; Te-rich (Se-poor) granular crystals were formed near the bottom half parts of the film and Te-poor (Se-rich) nanowires were formed at the upper half parts of the film. Columnar ZnSe crystals contain high-density {111} stacking faults due to the low stacking fault energy of ZnSe. A balance of deposition and re-evaporation on the substrate during the film growth will be responsible for the resultant nanocrystal morphology. *Published by AIP Publishing.* [http://dx.doi.org/10.1063/1.4964874]

## I. INTRODUCTION

Composite thin films of semiconductor nanocrystals embedded in a matrix have a potential application for quantum dot (QD) solar cells.[1] Semiconductor nanocrystals provide a shift in optical absorption edge due to quantum size effects, capable of tuning an optical gap to effective energy region for absorbing visible and near infrared light in the solar radiation spectrum.[2–6] A wide-gap semiconductor sensitized by QDs is a candidate material for such purpose. To produce a composite thin film with QDs, insolubility of sensitizer against a host semiconductor is indispensable. In this respect, the PbSe-ZnSe pseudobinary system is a possible candidate since the mutual solubility limit is less than 1 mol. % at temperatures below 1283 K.[7] In addition to the immiscible nature, the PbSe nanocrystals embedded in a ZnSe matrix is capable of exhibiting strong quantum confinement[8] because of the relatively large exciton Bohr radius of 46 nm in PbSe[9] and the relatively larger band gap difference between ZnSe (2.67 eV)[10] and PbSe (0.27 eV).[11] Wise reported that the degree of quantum confinement of charge carriers can be many times stronger than in most II–VI and III–V semiconductors.[9] Hence, the production of nanostructured PbSe via a simple route is of technical interest. One of the authors (S.A.) proposed a novel one-step synthesis method of composite thin film with the PbSe nanocrystals embedded in a ZnSe matrix using a hot-wall deposition (HWD) technique.[12] To improve several properties such as energy band gap, carrier concentration, and low temperature stability of QDs, the substitution of Se with Te was attempted in the preceding study.[13] As a result, the beginning of broad absorption was detected at the photon energy of 1 eV for a $PbTe_{1-x}Se_x$-ZnSe composite thin film, while pure ZnSe shows steep absorption edge at a relatively high photon energy of 2.65 eV. The observed broad absorption can be attributed to the nanometer-sized $PbTe_{1-x}Se_x$ crystals, while the structural details of the composite thin film still remain an open question.

The purpose of this study is to reveal the microstructure of $PbTe_{1-x}Se_x$-ZnSe composite thin films produced by the HWD method using scanning transmission electron microscopy (STEM) and electron diffraction. Improved resolution and chemical sensitivity of high-angle annular dark-field (HAADF) STEM imaging enable the atomic scale characterization of structural and chemical irregularities in the nanostructures.

## II. EXPERIMENT

Composite thin film was prepared using a homemade HWD apparatus composed of three electric furnaces, designated as hot-wall, source-1, and source-2.[12,13] The temperature of each could be controlled independently. The substrate temperature was kept at 340 K by circulating water. PbTe and ZnSe were used as evaporation sources with 5N purity. The PbTe and ZnSe sources were, respectively, located in the source-2 and source-1 furnaces for simultaneous evaporation to a glass substrate (Corning Eagle 2000). Here, the temperatures were kept constant at 683 K for the hot wall and 843 K for source-1 (ZnSe). The source-2 (PbTe) temperature was varied from 753 K to 793 K to provide a different PbTe content. The details of the HWD apparatus can be found in the literatures.[12,13]

[a)]Present address: Research Center for Ultra-High Voltage Electron Microscopy, Osaka University, Ibaraki 567-0047, Japan.

Specimens were thinned by focused ion beam (FIB) microsampling and Ar ion milling for electron transmittance. The microstructures of the specimens were characterized using a JEOL JEM-ARM200F STEM operating at 200 kV with a CEOS aberration corrector for the probe-forming lens and a cold field emission gun. We set the beam convergence to be ~23 mrad in the semi-angle. The HAADF-STEM images were acquired with the collection semi-angle of 68–175 mrad. The selected area electron diffraction (SAED) patterns were obtained from an area of $\sim 0.8\,\mu m^2$ and recorded using a charge coupled device camera (Gatan Orius200D). Intensity profiles of SAED patterns were obtained by integrating intensities in the circumference direction using a computer software.[14] Compositional analyses were carried out using an energy dispersive X-ray spectrometer (EDX; JEOL JED-2300) attached to the STEM equipped with a silicon drift detector. Quantitative EDX analyses were performed assuming theoretical k-factors for the thin film approximation method.[15]

## III. RESULTS

Figure 1(a) shows an SAED pattern and the intensity profile for a specimen deposited with the PbTe source temperature of 753 K. The beam incidence is in the film normal direction, namely, plan-view observation. The Debye-Scherer rings indicate the formation of a polycrystalline thin film. To identify crystal phases formed in the specimen, we have indexed the intensity profile measured from the SAED pattern. In Fig. 1(a), the intensity profile is indexed by two phases: PbSe with the NaCl structure and ZnSe with the zinc blend structure. It should be noted that binary PbSe is formed in spite of the deposition of PbTe and ZnSe due to vapor phase chemical reaction during the film growth. Figure 1(b) shows a representative EDX profile of the PbSe-ZnSe composite thin film. The absence of Te is also confirmed by a profile shown in the inset where the Te-K peak at 27.5 keV is missing. The reason for disappearance of Te during the film growth will be discussed later. The average composition derived from the EDX spectrum was $Pb_{12}Zn_{43}Se_{45}$ (at. %). A small peak of O, Si, and Ca come from the glass substrate.

Figure 2(a) shows an SAED pattern and the intensity profile for a specimen deposited with the PbTe source temperature of 793 K. Two kinds of $PbTe_{1-x}Se_x$ ternary phases, a Se-rich phase (termed as NaCl I) and a Te-rich phase (termed as NaCl II), are formed as well as ZnSe, in contrast to the results obtained for the film deposited with the source temperature of 753 K. The existence of Te was clearly detected by the STEM-EDX analysis, as shown in Fig. 2(b).

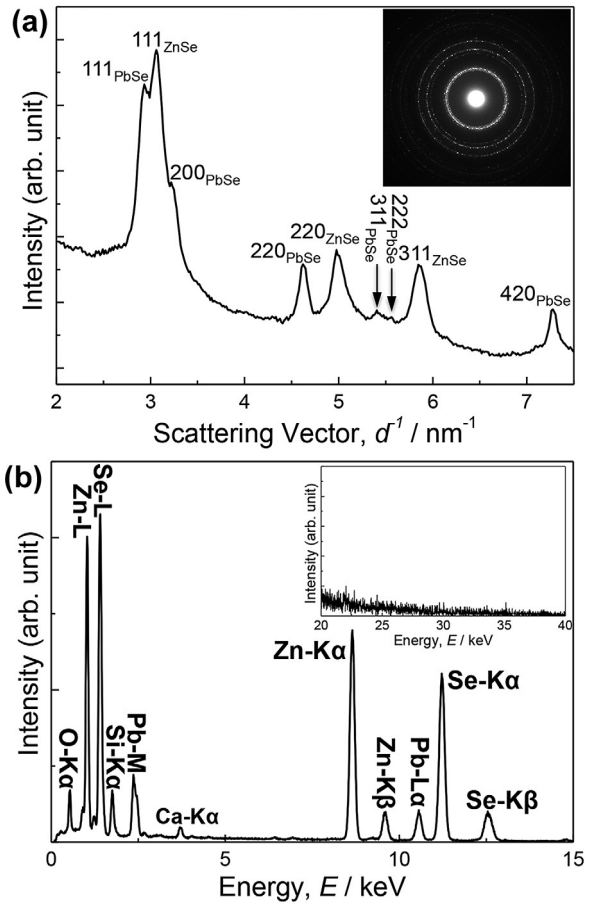


FIG. 1. (a) An SAED pattern and the intensity profile for a specimen deposited with the PbTe source temperature of 753 K. The beam incidence is in the film normal direction (plan-view). (b) A representative EDX profile of the PbSe-ZnSe composite thin film. Inset shows an EDX profile with energy range between 20 and 40 keV. Te-K peak at 27.5 keV is missing.

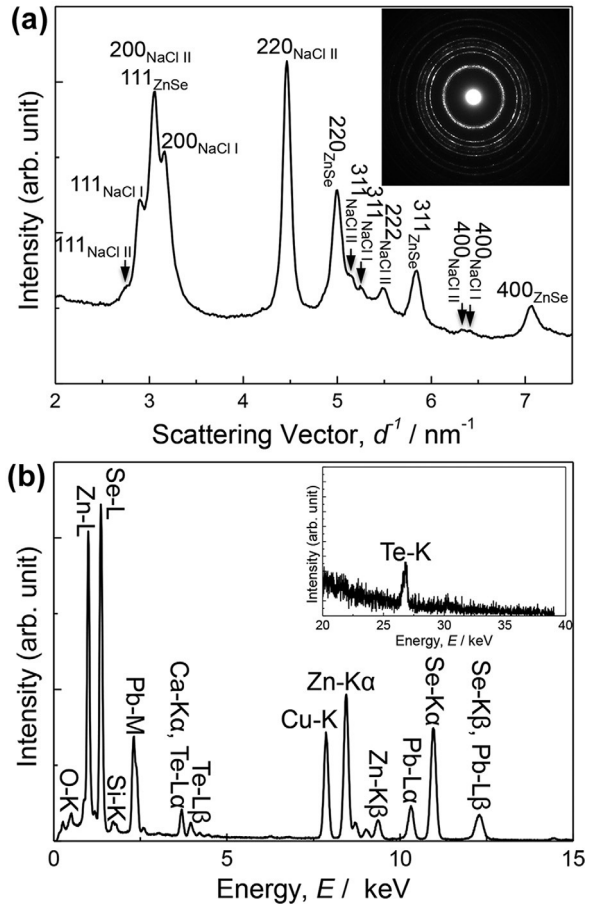


FIG. 2. (a) An SAED pattern and the intensity profile for a specimen deposited with the PbTe source temperature of 793 K. The beam incidence is in the film normal direction (plan-view). (b) A representative EDX profile of the PbSe-ZnSe composite thin film. Inset shows an EDX profile with energy range between 20 and 40 keV. Te-K peak at 27.5 keV is clearly seen.

The average composition derived from the EDX spectrum was $Pb_{11}Te_7Zn_{39}Se_{43}$ (at. %). The overall structural features of the thin films as a function of the PbTe source temperature are in accordance with the results obtained by the X-ray diffraction.[13]

Figures 3(a) and 3(b) show the plan-view HAADF-STEM images of PbSe-ZnSe and $PbTe_{1-x}Se_x$-ZnSe thin films, respectively. As can be seen, PbSe and $PbTe_{1-x}Se_x$ nanocrystals appear as bright contrast due to atomic number (Z) contrast of HAADF-STEM since Pb is the heaviest element among Pb (Z = 82), Te (Z = 52), Se (Z = 34), and Zn (Z = 30). In Fig. 3(a), the PbSe nanocrystals ~15 nm in sizes are distributed. The bright contrast region also distributes at grain boundaries of ZnSe matrix. Since pure Pb was not detected by the SAED analysis, as shown in Fig. 1(a), the bright contrast region at grain boundaries can be considered as the PbSe phase. In the case of $PbTe_{1-x}Se_x$-ZnSe thin film, nanocrystals are densely distributed and are partly connected with each other, forming a maze-like structure. The source temperature difference may affect such nanocrystal morphology.

Figure 4(a) shows an HAADF-STEM image of a representative PbSe nanocrystal surrounded by the ZnSe matrix.

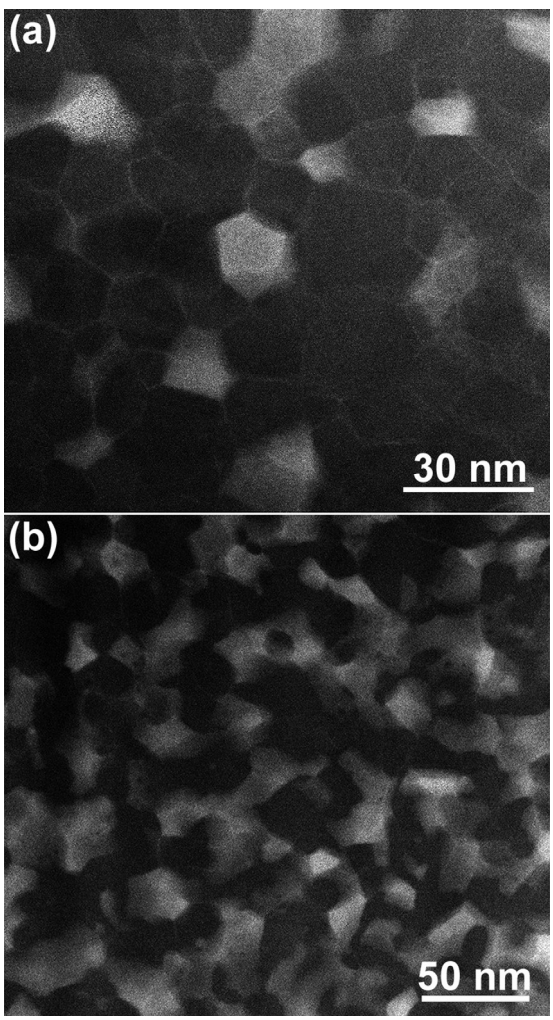


FIG. 3. Plan-view HAADF-STEM images of (a) PbSe-ZnSe and (b) $PbTe_{1-x}Se_x$-ZnSe thin films. PbSe and $PbTe_{1-x}Se_x$ nanocrystals are seen as bright contrast due to Z-contrast of HAADF-STEM.

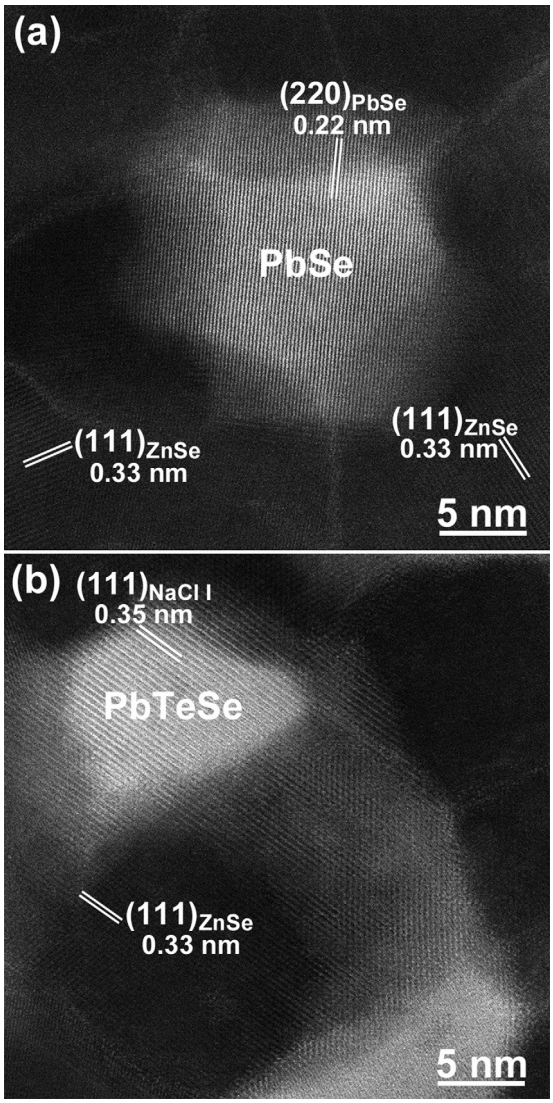


FIG. 4. Plan-view HAADF-STEM images of representative nanocrystals: (a) a PbSe nanocrystal and (b) a $PbTe_{1-x}Se_x$ (NaCl I) nanocrystal surrounded by ZnSe matrix.

As seen, a ~15 nm-sized PbSe nanocrystal shows irregular shape and the PbSe/ZnSe interface is not coherent. Similar tendency was obtained for $PbTe_{1-x}Se_x$ nanocrystals, as shown in Fig. 4(b). The Se-rich phase (NaCl I) can be distinguished from the Te-rich phase (NaCl II) by the lattice spacing as well as composition.

Figures 5(a) and 5(b) show the cross-sectional HAADF-STEM images of PbSe-ZnSe and $PbTe_{1-x}Se_x$-ZnSe thin films, respectively. In Fig. 5(a), PbSe nanocrystals, appear as bright contrast, grow in granular shape in the film bottom and then it changes to nanowire as the film grows. The nanowires are typically ~10 nm in diameter and ~100 nm in length. It should be mentioned that the ⟨111⟩ orientation was frequently observed in the longitudinal direction of PbSe nanowires, which was inclined by 5°–10° from the film growth direction. A representative image is shown in the inset of Fig. 5(a). The $PbTe_{1-x}Se_x$-ZnSe thin film shows similar variation of nanocrystal morphology, granule to nanowire, as shown in Fig. 5(b), while the areal density of ternary $PbTe_{1-x}Se_x$ nanocrystals is much higher than that of binary

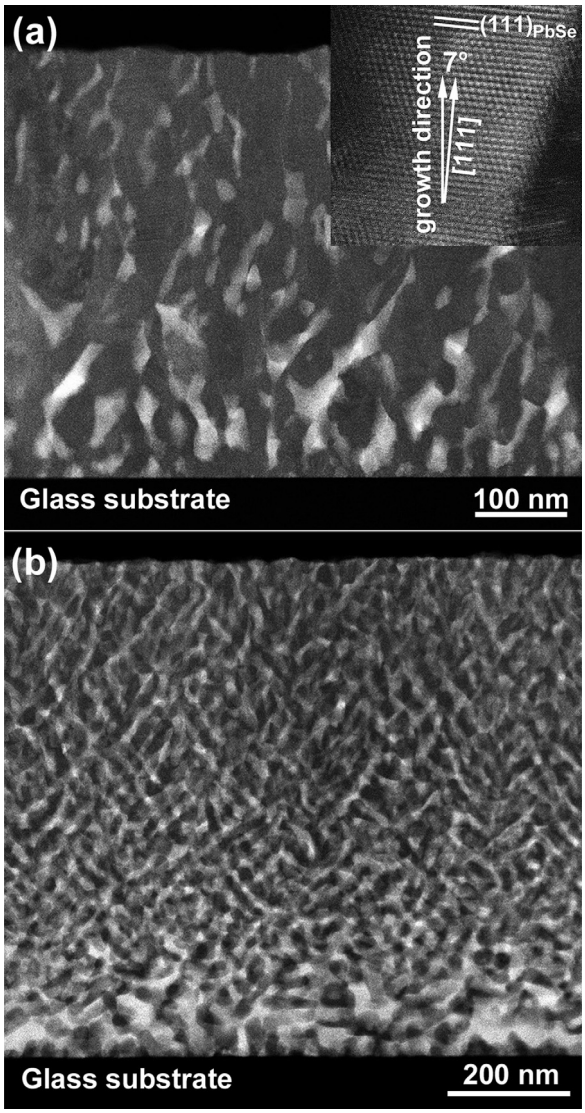


FIG. 5. Cross-sectional HAADF-STEM images of (a) PbSe-ZnSe and (b) $PbTe_{1-x}Se_x$-ZnSe thin films. A representative image of a PbSe nanowire with ⟨111⟩ orientation is shown in the inset of (a). The nanocrystals grow in granular shape at the initial stage of film growth, and the morphology changes to nanowire-shape as the film grows irrespective of the Te concentration.

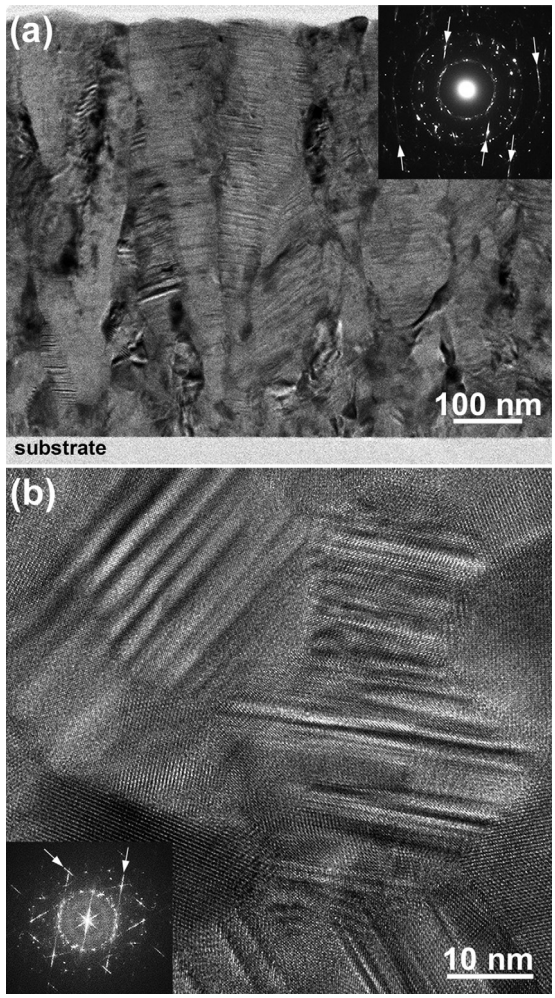


FIG. 6. (a) A cross-sectional BF-TEM image and the SAED pattern of the PbSe-ZnSe thin film. (b) A plan-view BF-TEM image and the corresponding FFT pattern of the PbSe-ZnSe thin film.

PbSe nanocrystals. The dense distribution of nanocrystals is in accordance with plan-view observation shown in Fig. 2(b). Overall, the morphology of PbSe and $PbTe_{1-x}Se_x$ nanocrystals shows granular structures at the bottom part of the films, while the nanowires are formed at the top half parts of the films.

Figure 6(a) shows a cross-sectional bright-field (BF) TEM image of the PbSe-ZnSe thin film. As seen, ZnSe grows like a columnar in shape. It was found that each column contains high-density {111} stacking faults, as evidenced by characteristic image contrast as well as streaks in the SAED pattern. Inclined streaks indicated by arrows are the evidence of inclination of ⟨111⟩ axis by 5°–10° from the film normal direction. Stacking faults are also seen in the plan-view image, as shown in Fig. 6(b). In this case, the stacking faults are not edge-on and hence the fringe contrasts are blurred. The fast Fourier transform (FFT) pattern of the image is shown in the inset. The angle among the streak patterns indicated by arrows is 60°, which can be explained by considering a tetrahedron composed of four kinds of {111} planes, namely, Thompson's tetrahedron.[16] The formation of high-density stacking faults can be attributed to the low stacking fault energy of ZnSe as low as 13 $mJ/m^2$.[17]

To understand the distribution of Te-rich and Se-rich $PbTe_{1-x}Se_x$ ternary phases that coexist in the $PbTe_{1-x}Se_x$-ZnSe thin film, we have performed STEM-EDX mapping. The average composition of the analyzed area was $Pb_{12}Te_9Zn_{37}Se_{42}$ (at. %). Figure 7(a) shows a Pb-M map that reproduces morphology variation of the $PbTe_{1-x}Se_x$ nanocrystals from the bottom to the top of the thin film. Te-L map shown in Fig. 7(b) revealed that the Te concentration is high at the bottom half parts of the film, while it is low at the upper part of the film. The Zn-K map (Fig. 7(c)) and the Se-K map (Fig. 7(d)) show almost homogeneous distribution of Zn and Se in the film, since these elements compose ZnSe matrix of the film. As a result, it was found that the granular shape $PbTe_{1-x}Se_x$ nanocrystals near the film bottom are enriched in Te, namely, PbTe phase including small amount of Se. The composition measured from the bottom half parts of the film was $Pb_{23}Te_{21}Zn_{26}Se_{30}$ (at. %). The composition can be rewritten as $Pb_{23}Te_{21}Se_4$-$Zn_{26}Se_{26}$, assuming a

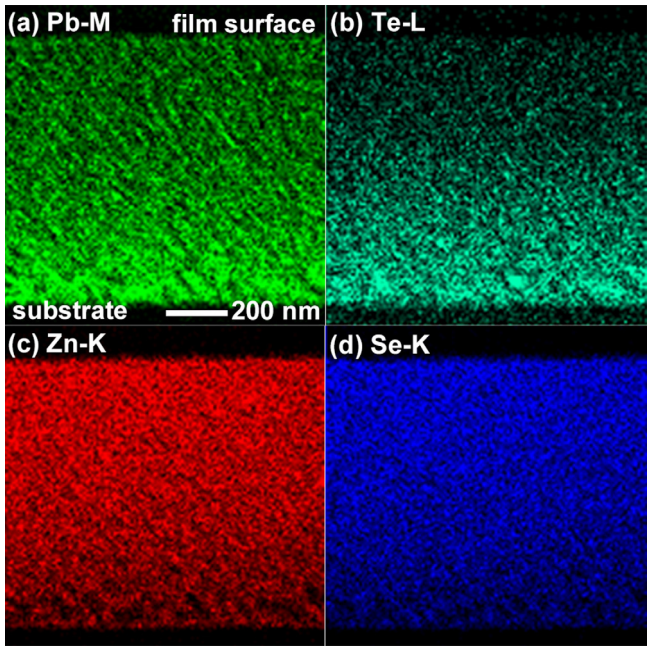


FIG. 7. Cross-sectional STEM-EDX elemental maps of the $PbTe_{1-x}Se_x$-ZnSe thin films: (a) Pb-M, (b) Te-L, (c) Zn-K, and (d) Se-K. Te-rich (Se-poor) granular crystals were formed near the bottom half parts of the film, and Te-poor (Se-rich) nanowires were formed at the upper half parts of the film.

stoichiometric composition of ZnSe, since PbTe and ZnSe are also immiscible with each other.[18] On the other hand, the nanowire shape nanocrystals at the upper part of the film are PbSe including small amount of Te. The composition measured from the top half parts of the film was $Pb_7Te_2Zn_{43}Se_{48}$ (at. %), namely, $Pb_7Te_2Se_5$-$Zn_{43}Se_{43}$.

## IV. DISCUSSION

Morphology change of nanocrystals, granule to nanowire, during the film growth is independent of Te concentration or PbTe source temperatures. It is presumed that such morphology change is originated from the film growth mechanism of the HWD method. In this process, deposition and re-evaporation of atoms are continuously repeated on the substrate surface, resulting in a state of near thermal equilibrium.[19] Once the shutter beneath the substrate is opened for deposition, substrate surface is exposed to radiation heat from the hot-wall, which may cause possible surface temperature raise and affect the aforementioned deposition and re-evaporation cycle. It is plausible that a possible heating effect by radiation can be enhanced at the later stage of film growth due to the accumulation of radiation heat; a balance of deposition and re-evaporation will be responsible for the resultant nanocrystal morphology.

In the HWD method, the concentrations of Te and Se in $PbTe_{1-x}Se_x$ can be controlled by the source temperature of PbTe.[13] The source temperature dependence of film composition can be briefly discussed as follows. First, in vapor phase, PbTe forms a binary compound,[20] while ZnSe dissociates to Zn and Se.[21] Hence, PbTe, Zn, and Se coexist in vapor phase. $PbTe_{1-x}Se_x$ nanocrystals and ZnSe matrix are formed via the following chemical reaction:[13]

$$\mathrm{PbTe(g)} + \mathrm{Zn(g)} + (1+x)/2\mathrm{Se_2(g)} \rightarrow \mathrm{ZnSe(s)} + \mathrm{PbTe_{1-x}Se_x(s)} + x/2\mathrm{Te_2(g)}. \quad (1)$$

The experimental results suggest that when the PbTe source temperature is low (753 K), the PbSe formation via the reaction of PbTe(g) and Se(g) is dominant and hence the Te concentration becomes less than the detection limit ($x \approx 0$), as shown in Fig. 1(b). It is presumed that desorbed Te was exhausted outside the HWD apparatus or condensed on a low temperature part of the apparatus. It is also noted that when the PbTe source temperature is high (793 K), the supply of PbTe is dominant at the initial stage of film growth, while the reaction of PbTe(g) and Se(g) becomes dominant at the later stage. A possible heating effect due to the radiation from the hot-wall may affect the above supply reaction balance; thin film growth at elevated substrate temperatures is our next step to control nanocrystal morphology. Thus, the HWD is a simple deposition method with a few experimental parameters, and hence it is suitable for one-step synthesis of PbTeSe-ZnSe nanocomposite thin films with good reproducibility and operability.

According to the preceding study, the beginning of broad absorption was detected at the photon energy of 1 eV for a $PbTe_{1-x}Se_x$-ZnSe composite thin film.[13] The observed broad absorption can be attributed to the distribution of nanocrystal size and shape of the PbSe and $PbTe_{1-x}Se_x$ phases. In the case of nanowires, diameter of ~10 nm is less than the exciton Bohr radius of 46 nm, while the 100 nm-sized long axis exceeds the exciton Bohr radius. Thus, nanocrystal size and shape limit the possible quantum confinement effect, and hence improvement of the nanocrystal morphology is necessary for realizing ideal quantum size effect. The effect of lattice strain on optical properties would be insignificant, since the PbSe/ZnSe interface is not coherent and overall film structure is polycrystalline.

## V. CONCLUSION

We have studied the microstructure of $PbTe_{1-x}Se_x$-ZnSe composite thin films using the STEM and electron diffraction. The results can be summarized as follows:

(1) Nanocrystals of $PbTe_{1-x}Se_x$ are formed in a ZnSe matrix. Tellurium concentration can be tuned by controlling the PbTe evaporation source temperatures between 753 K and 793 K. Binary PbSe nanocrystals were formed at 753 K, while ternary $PbTe_{1-x}Se_x$ nanocrystals were formed at 793 K.
(2) The nanocrystals grow in granular shape at the initial stage of film growth, and the morphology changes to nanowire-shape as the film grows irrespective of the Te concentration. A balance of deposition and re-evaporation on the substrate during the film growth will be responsible for the resultant nanocrystal morphology.
(3) Columnar ZnSe matrix crystals contain high-density {111} stacking faults due to the low stacking fault energy of ZnSe.
(4) The ternary $PbTe_{1-x}Se_x$ nanocrystals were composed of two phases with different Te concentration; Te-rich

(Se-poor) granular crystals were formed near the bottom half parts of the film, and Te-poor (Se-rich) nanowires were formed at the upper half parts of the film.

## ACKNOWLEDGMENTS

K.S. acknowledges Dr. Y. Kodama for the preparation of TEM specimens by the FIB microsampling.

[1]A. J. Nozik, Physica E **14**, 115 (2002).
[2]D. Liu and P. V. Kamat, J. Phys. Chem. **97**, 10769 (1993).
[3]P. Hoyer and R. Konenkamp, Appl. Phys. Lett. **66**, 349 (1995).
[4]S. Chatterjie, A. Goyal, and I. Shah, Mater. Lett. **60**, 3541 (2006).
[5]S. Abe, M. Ohnuma, D. H. Ping, and S. Ohnuma, Appl. Phys. Express **1**, 095001 (2008).
[6]G. Zhu, F. Su, T. Lv, L. Pan, and Z. Sun, Nanoscale Res. Lett. **5**, 1749 (2010).
[7]G. S. Oleinik, P. A. Mizetskii, and A. I. Nizkova, Inorg. Mater. **18**, 734 (1982).
[8]A. Lipovskii, E. Kolobkova, V. Petrikov, I. Kang, A. Olkhovets, T. Krauss, M. Thomas, J. Silcox, F. Wise, Q. Shen, and S. Kycia, Appl. Phys. Lett. **71**, 3406 (1997).
[9]F. W. Wise, Acc. Chem. Res. **33**, 773 (2000).
[10]S. Adachi and T. Taguchi, Phys. Rev. B **43**, 9569 (1991).
[11]J. N. Zemel, J. D. Jensen, and R. B. Schoolar, Phys. Rev. **140**, A330 (1965).
[12]S. Abe, Nanoscale Res. Lett. **6**, 324 (2011).
[13]S. Abe, Mater. Renewable Sustainable Energy **4**, 18 (2015).
[14]J. Labár, Microsc. Microanal. **14**, 287 (2008).
[15]G. Cliff and G. W. Lorimer, J. Microsc. **103**, 203 (1975).
[16]F. R. N. Nabarro, *Theory of Crystal Dislocations* (Dover, New York, 1987), p. 215.
[17]S. Takeuchi and K. Suzuki, Phys. Status Solidi A **171**, 99 (1999).
[18]V. I. Grytsiv, V. N. Tomashik, G. C. Olejnik, and Z. F. Tomashik, Izv. Akad. Nauk SSSR, Neorg. Mater. **16**, 543 (1980).
[19]A. Lopez-Otero, Thin Solid Films **49**, 3 (1978).
[20]R. F. Brebrick and A. J. Straus, J. Chem. Phys. **40**, 3230 (1964).
[21]P. Goldfinger and N. Jeunehomme, Trans. Faraday Soc. **59**, 2851 (1963).